ISSN (Online) : 2454 -7190 **ISSN (Print) 0973-8975**

Elasto-damage Modeling of Concrete Subjected to Proportionate and Non-proportionate Multiaxial State of Stress

[1]Asad-ur-Rehman Khan, [2]Tatheer Zahra

[1 2] Department of Civil Engineering, NED University of Engineering &Technology, University Road, Karachi, Sindh, Pakistan

[1] asadkhan@neduet.edu.pk, [2] tzahra77@yahoo.com

Corresponding Author: Asad-ur-Rehman Khan

Email: asadkhan@neduet.edu.pk

https://doi.org/10.26782/jmcms.2019.04.00002

Abstract

This study focuses on the improvement of predictive capabilities of elasto-damage model, initially proposed by Khan et al., for concrete subjected to multiaxial state of stress. The critical energy release rate R_c, which was initially assumed constant, is defined as a function of $f_c^{'}$, and E_o in the present study. Parameters α, β and γ used in effective compliance matrix, are redefined for the proposed form of R_c by regressing against available experimental data to obtain better estimates. The computer code for implementing the model is modified such that it is able to predict the response of concrete under both proportionate and non-proportionate loadings. The predictive capability of model to simulate stress-strain response of concrete subjected to multiaxial stresses and confining pressures is shown to have improved. The model is able to predict essential phenomenological behavior of concrete which relate well with the experimental results.

Keywords : Multiaxial stresses, Elasto-damage modeling, Confinement, Damage accumulation, Proportionate loading, Non-proportionate loading

I. Introduction

Modeling of mechanical behavior of concrete has been focus of considerable research in recent years due to the complex nature of concrete and variations in material characteristics. Typical trends in concrete behavior that needs to be considered while modeling concrete are stiffness degradation, strain softening, volumetric dilatation, different behavior in tension and compression, and gain in strength under increasing proportionate and non-proportionate confinement. A number of analytical models have been developed to predict behavior of concrete under triaxial stresses since 1980's

(Ahmad and Shah [XV], Wang *et al.* [III], Attard and Setunge [XIII], Imran and Pantazpoulou [X], Candappa*et al.* [IV], Lokuge*et al.* [XXI], Sfer*et al.* [V]). Models based on elasticity theory were not able to capture the strain softening and post peak behavior of concrete. More recently proposed models utilize general theories of solid mechanics including theory of plasticity, linear and non-linear fracture mechanics and damage mechanics.

Continuum damage mechanics has been extensively used to model the nonlinear behavior of concrete. Mechanical behavior of concrete subjected to multiaxial state of stress such as stiffness degradation, strain softening, volumetric dilatation etc., can be defined as a function of micro cracking and growth of micro cracks under increasing external loads. Babu*et al.* [XIV] while reviewing constitutive modeling of concrete have discussed various damage models that have been proposed to predict behavior of concrete using elastic damage(Ahmad and Shah [XV], Chen [XX]), plastic damage (Lee and Fenves. [XI]), bounding surface (Suaris*et al.* [XXII],Voyiadjis and Abu. Lebdeh [VII], Khan *et al.* [I]) and endochronic theory (Wu and Komarakulnanakorn [IX]).Continuum damage mechanics based models utilize either concepts from theory of plasticity or thermodynamic fundamentals and energy balance.

Khan *et al.* [I] have successfully used the concept of bounding surface defined in strain energy release rate and damage space to predict the essential features of normal and high strength concretes. In an attempt to improve predictive capability of the model, Khan and Naseem [II] defined the critical energy release rate R_c(a parameter used to model failure of concrete in bounding surface concept) as a function of $f_c^{'}$, and E_o instead of taking it as a constant as was the case in initially proposed model. Modified model was tested for uniaxial and biaxial stress paths and improved predicted response was observed.

Present work is an attempt to improve predictive capabilities of the model initially proposed by Khan *et al.* [I] and modified by Khan and Naseem [II] for multiaxial and biaxial states of stress respectively so that it may be used for both proportionate and non-proportionate multiaxial loading conditions. Parameters α, β and γ are redefined for the proposed form of R_c by regressing against available experimental data to obtain better estimates. The predictive capability of model to simulate stress-strain response of concrete under triaxial stresses and confining pressures is shown to have improved. The model is able to predict essential phenomenological behavior of concrete such as stiffness degradation, strain softening, increase in strength under confinement, failure strength envelope, volumetric dilatation and damage accumulation. Predictions of model are in good agreement with the experimental results.

II. Elasto-Damage Model

Theoretical aspects of this work are embedded in a damage model presented by Khan *et al.*[I]. Brief features of the model are presented here. Fundamental surfaces are defined in strain energy release space (originally presented in Suaris*et al.*[XXII]).

$$f = (R_i R_i)^{1/2} - R_c / b = 0 \tag{1}$$

$$F = (\bar{R}_i \bar{R}_i)^{1/2} - R_c = 0 \tag{2}$$

$$f_o = (R_i R_i)^{1/2} - R_o = 0 \tag{3}$$

where, f is the loading function surface, F is the bounding surface, f_o is a limit fracture surface.

The loading function surface f is defined in terms of thermodynamic-force conjugates, R_i, where,

$$R_i = \rho \frac{\partial \Lambda}{\partial \omega_i} (\sigma_{ij}, \omega_i) \tag{4}$$

Where ω_i, i = 1, 2, 3 are principal damage components. Also, $\rho\Lambda$ is the complementary energy density with ρ being the mass density.

$\bar{R}_i$ is an image point on F = 0 associated with a given point R_i on f = 0 defined by a mapping rule

$$\bar{R}_i = bR_i \tag{5}$$

$$b = R_c / (R_i R_i)^{1/2} \tag{6}$$

with the mapping parameter b ranging from an initial value of ∞ to a limiting value of 1 on growth of the loading surface to coalesce with the bounding surface. R_c, the critical strain energy release rate, is a parameter of the model that is calibrated to the standard uniaxial compression test.

Damage is hypothesized to accumulate at levels of strain energy release rate resulting in the loading surface f traversing the limit fracture surface f_o and rupture in the damage sense is said to occur when f grows large enough to coalesce with the bounding surface F fixed in the R_i space. For damaged materials, the constitutive equation may be expressed as

$$\varepsilon = \frac{\partial \Lambda(\sigma, \omega)}{\partial \sigma} = \tilde{C}(E(\omega), \nu(\omega))\sigma \tag{7}$$

where $\tilde{C}$ is the effective compliance matrix for damaged material in the principal coordinate system and σ is the stress vector in the principal coordinate system. E is the elastic modulus and ν is the Poisson's ratio. The complementary energy of a damaged material can be expressed as

$$\Lambda(\sigma,\omega)=\frac{1}{2}\sigma^{T}:\tilde{C}:\sigma \tag{8}$$

Based on physical insight and phenomenological evidence, the following elements of the compliance matrix $\tilde{C}$ are postulated in the principal coordinate system. Details of $\tilde{C}$can be found in [I] in which α,β,γ are calibrated parameters to account for phenomenologically known peak strengths and volumetric dilatation and E_o is the initial elastic modulus.

Four model parameters namely R_c (Critical Energy release rate), α (for tension state), β (for compression state) and γ (for volumetric change) are modified in this study by calibrating against available experimental data and incorporated in computer code EDMON3D that takes care of both proportionate and non-proportionate stress paths.

III. Regression of Model Parameters

The parameters $\boldsymbol{\alpha}$ and $\boldsymbol{\beta}$ control the damage growth rate and influence the pre- and post-peak behavior as well as the level at which the peak stress is attained. Thus, the behavior of concrete of varying compressive strength is simulated by different values ofα andβ. The parameters $\boldsymbol{\alpha,\beta,}$**and** $\boldsymbol{\gamma}$ are defined as functions of initial modulus of elasticity E_o, uniaxial compressive strength $\boldsymbol{f_c^{'}}$, and normalized strain invariants $\boldsymbol{I_1/\varepsilon_3}$ and $\boldsymbol{J_2^{'}/e_3^2}$, where $\boldsymbol{I_1=\varepsilon_{ii}}$ is the first invariant of strain tensor and $\boldsymbol{J_2^{'}=1/2e_{ij}e_{ij}}$is the second invariant of the deviatoric strain tensor. Here $\varepsilon_3$and e_3 represent the minor principal and deviatoric strain, respectively. Phenomenological evidence is the essential guide in deciding if a particular stress state corresponds to a path dependent or path independent loading.

Suggested forms of $\boldsymbol{\alpha,\beta,}$**and** $\boldsymbol{\gamma}$ are as follows:

- For path-dependent stress states

($\sigma_1>0$, $\sigma_2>0$, $\sigma_3<0$ and $\sigma_1>0$, $\sigma_2<0$, $\sigma_3<0$)

$$\boldsymbol{\alpha=\alpha_o(f_c',E_o)+\alpha_1\left(f_c^{'},E_o\right)\times\frac{I_1}{\varepsilon_3}+\alpha_2\left(f_c^{'},E_o\right)\times\frac{J_2^{'}}{e_3^2}+\alpha_3\left(f_c^{'},E_o\right)\times\frac{I_1}{\varepsilon_3}\times\frac{J_2^{'}}{e_3^2}} \tag{9}$$

($\sigma_1>0$, $\sigma_2<0$, $\sigma_3<0$ and $\sigma_1<0$, $\sigma_2<0$, $\sigma_3<0$)

$$\boldsymbol{\beta=\beta_o(f_c',E_o)+\beta_1\left(f_c^{'},E_o\right)\times\frac{I_1}{\varepsilon_3}+\beta_2\left(f_c^{'},E_o\right)\times\frac{J_2^{'}}{e_3^2}+\beta_3\left(f_c^{'},E_o\right)\times\frac{I_1}{\varepsilon_3}\times\frac{J_2^{'}}{e_3^2}} \tag{10}$$

Where,

$$\boldsymbol{\alpha_i=\alpha_{i1}+\alpha_{i2}\times f_c^{'}+\alpha_{i3}\times E_o+\alpha_{i4}\times E_o\times f_c^{'}(i=0,1,2,3)} \tag{11}$$

$$\boldsymbol{\beta_i=\beta_{i1}+\beta_{i2}\times f_c^{'}+\beta_{i3}\times E_o+\beta_{i4}\times E_o\times f_c^{'}(i=0,1,2,3)} \tag{12}$$

- For path-independent stress states

$$\boldsymbol{\alpha=\bar{\alpha}(f_c',E_o)(\sigma_1>0,\ \sigma_2>0,\ \sigma_3>0)}$$

$$\boldsymbol{\beta} = \overline{\boldsymbol{\beta}}(\boldsymbol{f_c}', \boldsymbol{E_o})(\boldsymbol{\sigma_1} > \mathbf{0},\ \boldsymbol{\sigma_2} > \mathbf{0},\ \boldsymbol{\sigma_3} < \mathbf{0}) \tag{13}$$

$$\boldsymbol{\gamma} = \boldsymbol{\gamma}\,(\boldsymbol{f_c}', \boldsymbol{E_o})(\boldsymbol{\sigma_1} < \mathbf{0},\ \boldsymbol{\sigma_2} < \mathbf{0},\ \boldsymbol{\sigma_3} < \mathbf{0})$$

Where,

$$\begin{aligned}
\overline{\boldsymbol{\alpha}} &= \overline{\boldsymbol{\alpha_o}} + \overline{\boldsymbol{\alpha_1}} \times \boldsymbol{f_c}' + \overline{\boldsymbol{\alpha_2}} \times \boldsymbol{E_o} + \overline{\boldsymbol{\alpha_3}} \times \boldsymbol{E_o} \times \boldsymbol{f_c}' \\
\overline{\boldsymbol{\beta}} &= \overline{\boldsymbol{\beta_o}} + \overline{\boldsymbol{\beta_1}} \times \boldsymbol{f_c}' + \overline{\boldsymbol{\beta_2}} \times \boldsymbol{E_o} + \overline{\boldsymbol{\beta_3}} \times \boldsymbol{E_o} \times \boldsymbol{f_c}' \\
\boldsymbol{\gamma} &= \boldsymbol{\gamma_o} + \boldsymbol{\gamma_1} \times \boldsymbol{f_c}' + \boldsymbol{\gamma_2} \times \boldsymbol{E_o} + \boldsymbol{\gamma_3} \times \boldsymbol{E_o} \times \boldsymbol{f_c}'
\end{aligned} \tag{14}$$

These parameters were calibrated for different concrete strengths as given in Table 1.

Table 1. Range of f_c' used in Monotonic Loading

f_c' (psi, MPa)	E_o($\times 10^6$ psi)
4000, 27	3.605 [VI]
6531, 45	5.460 [XVIII]
9434, 65	6.023 [XVIII]
13062, 90	6.444 [XVIII]
17416, 120	7.126 [XVIII]

Stress paths used in regression of path dependent $\boldsymbol{\alpha}$ and $\boldsymbol{\beta}$ can be found in reference [I]. For determination of $\boldsymbol{\gamma_i}$'s regression was done only once due to its dependence on $\boldsymbol{f_c}'$ and $E_o$only.

Final forms of parameters given below are unit sensitive and "psi" should be used for $\boldsymbol{f_c}'$ and $E_o$in evaluating these parameters:

• $\boldsymbol{\alpha}, \boldsymbol{\beta}$ **and** $\boldsymbol{\gamma}$ for ($\sigma_1 > 0$, $\sigma_2 \geq 0$, $\sigma_3 \geq 0$) [Tension-Tension-Tension]

$$\boldsymbol{\alpha} = 26.5563 - 2.9282\text{E-}03 \times \boldsymbol{f_c}' - 2.5423\text{E-}06 \times E_o + 3.55154\text{E-}10 \times \boldsymbol{f_c}' \times E_o \tag{15}$$

$$\boldsymbol{\alpha} = 0 \text{ and } \boldsymbol{\gamma} = 0 \tag{16}$$

• $\boldsymbol{\alpha}, \boldsymbol{\beta}$ **and** $\boldsymbol{\gamma}$ for ($\sigma_1 > 0$, $\sigma_2 \geq 0$, $\sigma_3 < 0$) [Tension-Tension-Compression]

$$\begin{aligned}
\boldsymbol{\alpha_0} &= -3.324\text{E+}01 + 2.348\text{E-}03 \times \boldsymbol{f_c}' + 4.060\text{E-}06 \times E_o - 3.057\text{E-}10 \times \boldsymbol{f_c}' \times E_o \\
\boldsymbol{\alpha_1} &= -2.701\text{E+}01 + 4.589\text{E-}03 \times \boldsymbol{f_c}' + 1.992\text{E-}06 \times E_o - 5.570\text{E-}10 \times \boldsymbol{f_c}' \times E_o \\
\boldsymbol{\alpha_2} &= 5.540\text{E+}01 - 5.375\text{E-}03 \times \boldsymbol{f_c}' - 6.053\text{E-}06 \times E_o + 6.776\text{E-}10 \times \boldsymbol{f_c}' \times E_o \\
\boldsymbol{\alpha_3} &= 1.989\text{E+}01 - 2.641\text{E-}03 \times \boldsymbol{f_c}' - 1.845\text{E-}06 \times E_o + 3.262\text{E-}10 \times \boldsymbol{f_c}' \times E_o
\end{aligned} \tag{17}$$

and

$\boldsymbol{\beta}$ = 0.643665 – 4.69309E−05× $\boldsymbol{f_c'}$ − 7.71E-08×E_o+ 6.022E-12× $\boldsymbol{f_c'}$ ×E_o (18)

and $\boldsymbol{\gamma}$ = 0

• $\boldsymbol{\alpha, \beta}$ **and** $\boldsymbol{\gamma}$for ($\sigma_1 \geq 0$, $\sigma_2 < 0$, $\sigma_3 < 0$) [Tension- Compression-Compression]

$\boldsymbol{\alpha_0}$= 7.8048E+01–6.0063E-03×$\boldsymbol{f_c'}$ –8.6958E-06×E_o+7.4951E-10× $\boldsymbol{f_c'}$×E_o

$\boldsymbol{\alpha_1}$= –7.1203E+01+5.4640E-03× $\boldsymbol{f_c'}$+7.9321E-06×E_o–6.8166E10× $\boldsymbol{f_c'}$×E_o (19)

$\boldsymbol{\alpha_2}$= –1.4338E+01+1.2332E-03×$\boldsymbol{f_c'}$ +1.5109E-06×E_o–1.5119E-10× $\boldsymbol{f_c'}$×E_o

$\boldsymbol{\alpha_3}$= 1.6029E+01–1.3101E-03× $\boldsymbol{f_c'}$–1.7334E-06×E_o+1.6182E-10× $\boldsymbol{f_c'}$×E_o

and

$\boldsymbol{\beta_0}$= 9.9351E-01– 6.5957E-05× $\boldsymbol{f_c'}$ – 1.2277E-07×E_o+8.6393E-12× $\boldsymbol{f_c'}$×E_o

$\boldsymbol{\beta_1}$= –1.5283E-01+1.3190E-05× $\boldsymbol{f_c'}$+1.5177E-08×E_o+1.5719E-12× $\boldsymbol{f_c'}$×E_o

$\boldsymbol{\beta_2}$= –5.0825E-01+ 2.1187E-05× $\boldsymbol{f_c'}$ + 7.2680E-08 x E_o–3.2310E-12× $\boldsymbol{f_c'}$×E_o (20)

$\boldsymbol{\beta_3}$= 2.7165E-01–1.1523E-05 ×$\boldsymbol{f_c'}$ – 3.8623E-08×E_o+1.7450E-12× $\boldsymbol{f_c'}$×E_o

and $\boldsymbol{\gamma}$ = 0

• $\boldsymbol{\alpha, \beta}$ **and** $\boldsymbol{\gamma}$ for ($\sigma_1 \leq 0$, $\sigma_2 < 0$, $\sigma_3 < 0$) [Compression- Compression-Compression]

$\boldsymbol{\alpha}$ = 0 (21)

And if ($\sigma_1 = 0$, $\sigma_2 < 0$, $\sigma_3 < 0$) [Biaxial Compression]

$\boldsymbol{\beta_0}$= 9.9351E-01– 6.5957E-05 ×$\boldsymbol{f_c'}$ – 1.2277E-07 × E_o+ 8.6393E-12 × $\boldsymbol{f_c'}$ × E_o

$\boldsymbol{\beta_1}$= –1.5283E-01 + 1.3190E-05 × $\boldsymbol{f_c'}$+1.5177E-08 × E_o+ 1.5719E-12 × $\boldsymbol{f_c'}$ ×E_o

$\boldsymbol{\beta_2}$= –5.0825E-01 + 2.1187E-05 × $\boldsymbol{f_c'}$ + 7.2680E-08 x E_o– 3.2310E-12 × $\boldsymbol{f_c'}$ × E_o (22)

$\boldsymbol{\beta_3}$=2.7165E-01 – 1.1523E-05 × $\boldsymbol{f_c'}$ – 3.8623E-08 × E_o+ 1.7450E-12 × $\boldsymbol{f_c'}$ × E_o

and

$\boldsymbol{\gamma}$ = 3.1344–1.1826E-4× $\boldsymbol{f_c'}$ – 2.903E-07×E_o+1.28434E-11× $\boldsymbol{f_c'}$×E_o (23)

Else if ($\sigma_1 < 0$, $\sigma_2 < 0$, $\sigma_3 < 0$) [Triaxial Compression]

$\boldsymbol{\beta_0}$= –3.3154E-01 + 1.7819E-05× $\boldsymbol{f_c'}$ + 4.7389E-08 ×E_o – *2.6098E*-12× $\boldsymbol{f_c'}$×E_o

$\boldsymbol{\beta_1}$ = 1.5023E-01 – 8.0370E-06 ×$\boldsymbol{f_c'}$ – 2.1507E-08×E_o +1.1791E-12× $\boldsymbol{f_c'}$×E_o

$\boldsymbol{\beta_2}$= 6.1909E-01 –3.2969E-05× $\boldsymbol{f_c'}$ 8.8906E-08x E_o+ 4.8527E-12× $\boldsymbol{f_c'}$×E_o (24)

$\boldsymbol{\beta_3}$= –3.4059E-01 + 1.8123E-05× $\boldsymbol{f_c'}$ + *4.8917*E-08×E_o– 2.6679E-12× $\boldsymbol{f_c'}$×E_o

and $\boldsymbol{\gamma}$ = 0

IV. Results and Discussion

EDMON3D was employed to predict the static behavior of concrete subjected to multiaxial state of stress. Predictions and results are presented in the form of stress-strain curves, volumetric dilatation, biaxial strength interaction envelopes, comparison of peak strengths and damage accumulation. Predictions of the model are compared against experimental data and predictions of previous model [I]. Properties of concrete used are listed in Table 2.

Table 2. Properties of Concrete used

Concrete	f_c' (psi, MPa)	E_o(x 10^6 psi)	ν
A[VI]	4000, 27	3.605	0.19
B[XVIII]	9434, 65	6.023	0.19
C[XVIII]	17416, 120	7.126	0.19
D[XVII]	10504, 72	5.905	0.19
E[XVII]	13659, 94	6.708	0.19
F[XVII]	6683, 46	4.692	0.19
G [XVI]	4351, 30	3.760	0.19
H [XIX]	6364, 44	4.952	0.19
J [VIII]	4650, 32	4.400	0.20

Predictive capabilities of the model were tested for the following states of stress:

Uniaxial Compression ($\boldsymbol{\sigma_1}$ = 0, $\boldsymbol{\sigma_2}$= 0, $\boldsymbol{\sigma_3}$)

Biaxial Compression ($\boldsymbol{\sigma_1}$ = 0, $\boldsymbol{\sigma_2}$=$\boldsymbol{r_1\sigma_3}$, $\boldsymbol{\sigma_3}$)

Uniaxial Tension ($\boldsymbol{\sigma_1}$,$\boldsymbol{\sigma_2}$= 0, $\boldsymbol{\sigma_3}$= 0)

Tension-Compression ($\boldsymbol{\sigma_1}$ = - $\boldsymbol{r_2\sigma_3}$, $\boldsymbol{\sigma_2}$= 0, $\boldsymbol{\sigma_3}$)

Tension-Compression-Compression ($\boldsymbol{\sigma_1}$ = - $\boldsymbol{r_2\sigma_3}$, $\boldsymbol{\sigma_2}$= - $\boldsymbol{r_1\sigma_3}$, $\boldsymbol{\sigma_3}$)

Triaxial Compression ($\boldsymbol{\sigma_1}$ = $\boldsymbol{r_2\sigma_3}$, $\boldsymbol{\sigma_2}$= $\boldsymbol{r_1\sigma_3}$, $\boldsymbol{\sigma_3}$)

Where $\boldsymbol{r_i}$ ($\boldsymbol{i}$ = 1,2) are appropriate principal stress ratios. $\boldsymbol{r_i}$is constant for proportionate loading while it varies at every increment in case of non-proportionate loading.

Uniaxial Compression

For the case of uniaxial compression, predictions are compared with the experimental results and that of Khan *et al.*[I] in terms of peak stress, stress-strain response and volumetric dilatation. Stress-strain curves are compared in Fig.1 for three different concretes i.e. A, B, and C with experimental results of Wischers[VI], Wee *et al.*[XVIII] and Khan *et al.*[I]. It can be seen in Fig.1 that results compare well with the experimental results in terms of peak stress but are bit stiffer in post peak response for concrete A and B. Comparison of the results with the previous model of Khan *et al.*[I],

shows improvement in the predicted response of the current model in terms of softening in both pre-and post-peak response.

Predictive capability of the model to capture the phenomenological behavior of volumetric dilatation is shown in Fig.2. It can be seen that dilatancy caused by the increase in lateral strains as the stress reaches the peak stress has been captured effectively and the predicted volumetric strain conforms well with the experimental data of Kupfer*et al.*[VIII]. This increase in lateral strains is due to the dramatic increase in apparent Poisson's ratio, which results in the change of sign of dilatancy (volumetric strain). This change in Poisson's ratio is presented in Fig.3 which reflects the capability of the model to pick the exponential change in Poisson's ratio when stress is close to peak stress. Comparison with previous model in Fig.3 shows improvement in results of the current model.

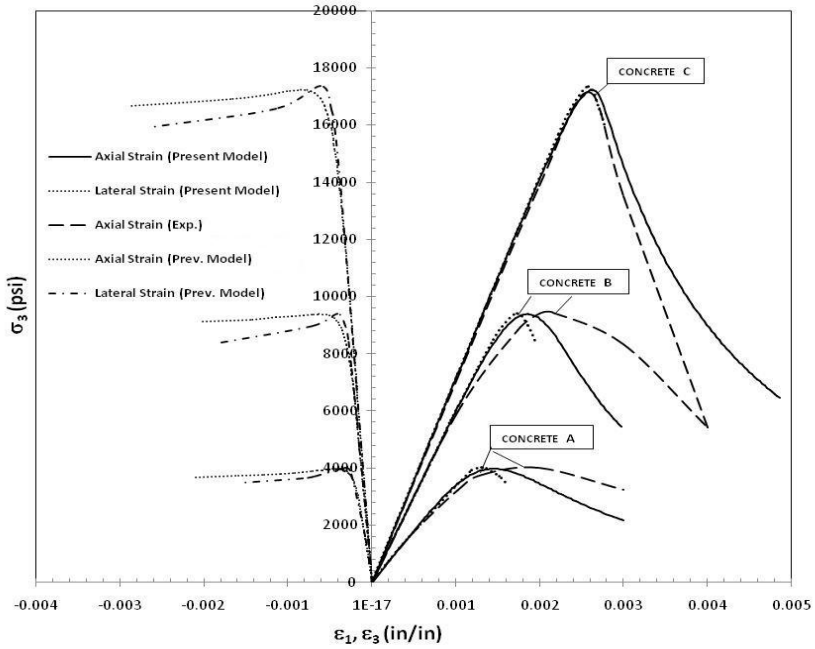

Figure 1.Comparison of Stress Strain Curve of Concretes A, B & C for Uniaxial Compression with Khan *et al.*[I] and Experimental data [VI,XVIII]

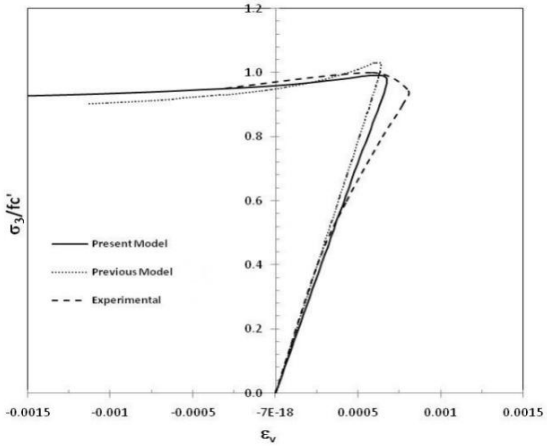

Figure 2.Volumetric Dilatation of Concrete B under Uniaxial Compression

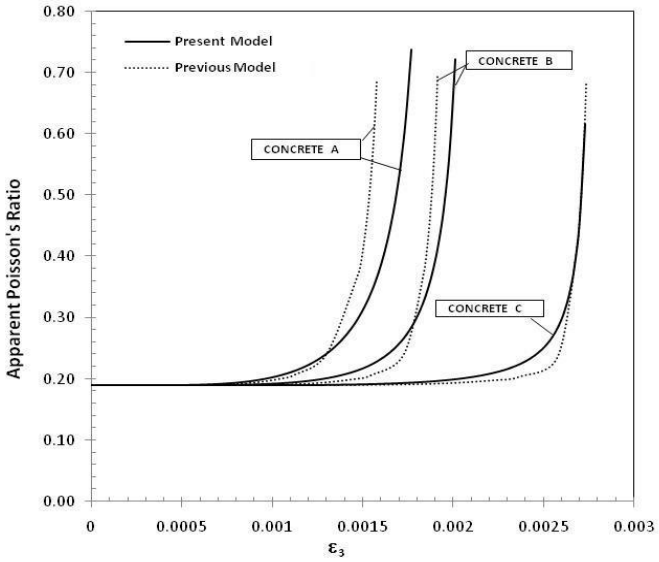

Figure 3.Apparent Poisson's Ratio – Uniaxial Compression, Comparison with Previous Model of Khan *et al.*[I]

Biaxial Compression [C-C]

For the case of biaxial compression, model predictions are compared with the experimental results and that of Khan *et al.*[I] in terms of biaxial strength interaction envelope and volumetric dilatation. In Fig.4 biaxial strength interaction envelope is compared with the experimental results of Kupfer*et al.*[VIII] which compares well with Kupfer*et al.*'s envelope. Experimental results of Hampel *et al.*[XVII] were also validated for concrete under biaxial compression. Comparison of model predictions and

experimental results is shown in Fig.5 for concretes D and E. Predictions of model are quite comparable with those obtained from experiments. Differences may be attributed towards the fact that model has been calibrated using experimental results of Kupfer*et al.*[VIII] which is reflected in Fig.4 where predicted envelope is almost matching with the experimental one.

Fig.6 shows the capability of the model to predict the phenomena of volumetric dilatation for various stress paths. It can be seen that beyond the onset of damage the rate of volume change increases until at 80% - 90% of the ultimate, a point of inflection is reached. The minimum volume corresponding to the point of inflection occurs at about 95% of the peak stress. Further straining leads to the volumetric dilatation i.e. negative volumetric strains. Similar trend was observed in predictions of previous and modified models.

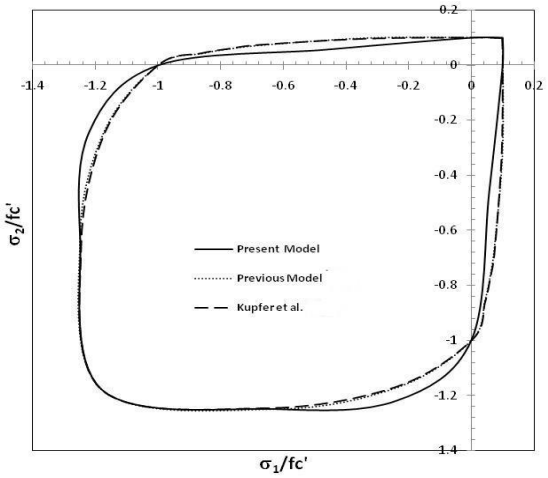

Figure 4. Biaxial Compression Interaction Envelope for Concrete A

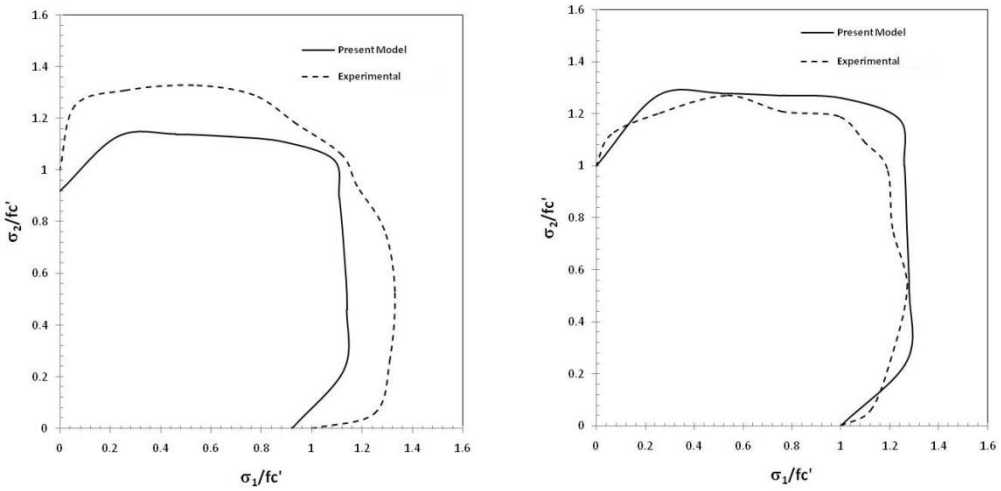

Figure 5.Failure Strengths in Biaxial Compression for Concretes D and E

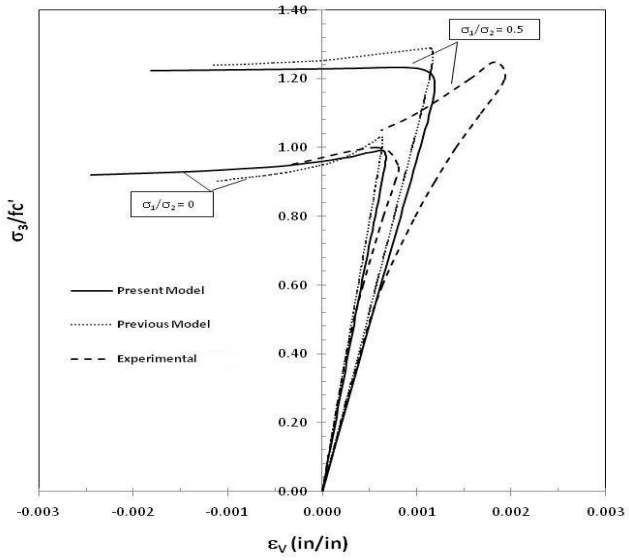

Figure 6.Volumetric Dilatation of Concrete A under Biaxial Compression

Triaxial Compression [C-C-C]

For the case of triaxial compression results are discussed in the following sections separately for the cases of proportionate and non-proportionate loadings.

Proportionate Loading: For the case of triaxial compression under proportionate loading, predictions are compared in terms of peak stress with the experimental results of Hampel*et al.* [XVII]. Comparison of predicted failure strengths with that of experimental ones is shown in Fig.7. It can be noticed that for stress ratio $\boldsymbol{\sigma_2/\sigma_1}$= 0.95, predicted failure strengths are quite comparable with experimentally defined failure strengths at all stress ratios of $\boldsymbol{\sigma_3/\sigma_1}$ (0.05, 0.1, 0.15). Whereas, peaks are differing a little bit for other stress ratios of $\boldsymbol{\sigma_2/\sigma_1}$ (0.2, 0.6). This again may be attributed to the fact that calibration of parameter $\boldsymbol{\beta}$ was carried out using different set of experimental results and concrete strengths available in the literature. This difference in peak strengths can be reduced by using a large number of experimental data in calibrating model parameters.Experiments results of Gabet*et al.*[XVI] for concrete subjected to proportionate triaxial loading are also validated from the present model. Comparison of peak values is shown in Fig. 8. A very close comparison can be noticed between the predicted and experimental peaks.

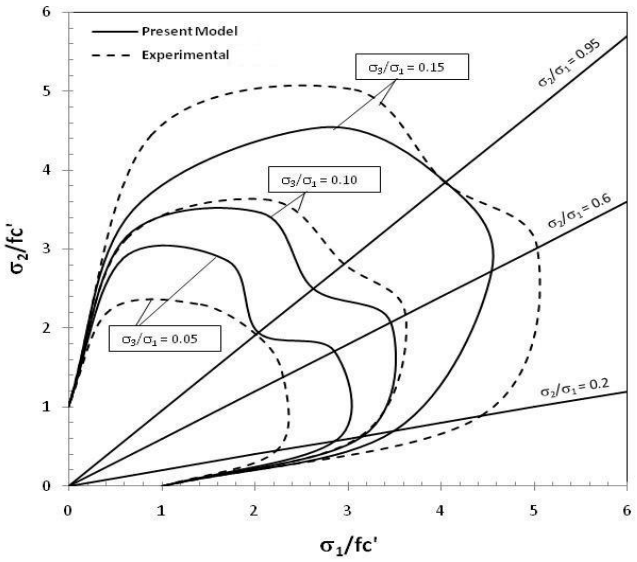

Figure 7. Failure Strengths in Triaxial Compression for Concrete F

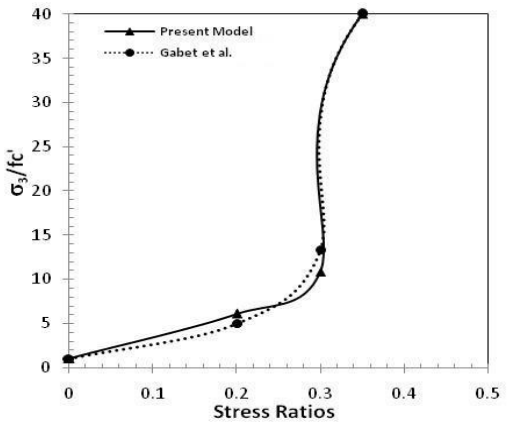

Figure 8. Peak Strengths in Triaxial Compression for Varying Stress Ratios (Concrete G)

Non-Proportionate Loading: Most of the experimental data available in literature related to triaxial testing of concrete is for non-proportionate loading. In non-proportionate triaxial testing, axial load is applied to the specimen at constant confining pressure. Some experimental results where concrete is subjected to non-proportionate traixial loading have also been compared with the model predictions. The experimental work of Gabet*et al.*[XVI] and Sfer*et al.* [V] are used to compare peak strengths as predicted by the model. These are shown in Tables 3 and 4. It can be seen from the Tables that model predictions are on the higher side as compared to the experimental results especially when confining pressure is very high. This might be due to the fact that parameter $\boldsymbol{\beta}$ is calibrated using the data at low confining pressures. Results for non-proportionate loading can further be improved by incorporating more experimental data in calibration of $\boldsymbol{\beta}$.

Table 3. Comparison of Peak Strengths $f_c^{'}$ = 30 MPa (Gabet et al. [XVI])

Confinement Pressure (MPa)	$\sigma_3/f_c^{'}$ (Model)	$\sigma_3/f_c^{'}$ (Exp.)
0	0.98	1.00
50	7.08	6.67
100	11.07	11.67
200	8.81	21.67
500	21.24	40.00
650	27.60	53.30

Table 4. Comparison of Peak Strengths $f_c^{'}$ = 33 MPa (Sfer et al. [V])

Confinement Pressure (MPa)	$\sigma_3/f_c^{'}$ (Model)	$\sigma_3/f_c^{'}$ (Exp.)
0	0.955	1.00
1.5	3.59	1.59
4.5	3.74	1.94
9.0	3.98	2.19
30.0	5.22	4.31
60.0	7.22	6.84

Uniaxial Tension: For the case of uniaxial tension, predicted stress-strain response and change in Poisson's ratio are compared with the experimental results of Gopalaratnam and Shah [XIX]. Stress-Strain curves are plotted for Concretes A, B and H in Fig.9. Softening in post-peak zone of stress strain plots for all concretes has been captured effectively. Predicted curves correlates well with the experimental results except that the peak stress from the model is on higher side which is due to the fact that experimental results corresponds to tensile strength $\boldsymbol{f_t}$of approximately *0.08*$\boldsymbol{f_c^{'}}$, whereas model has been calibrated to experimental data using $\boldsymbol{f_t = 0.1 f_c^{'}}$.

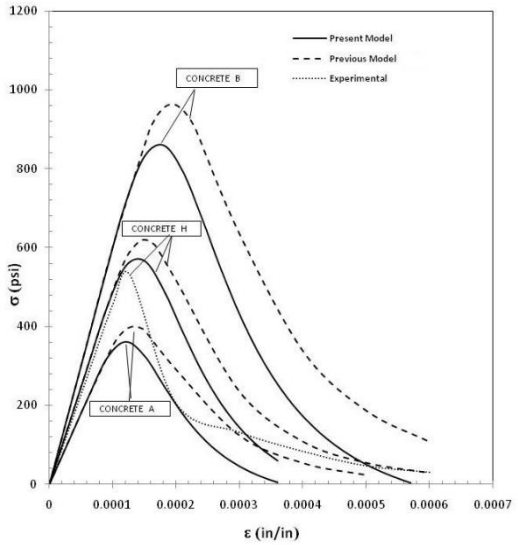

Figure 9. Stress-Strain Curve for Uniaxial Tension for Different Concretes

*Tension Compression (T-C):*For combined tension and compression, predictions are compared with the experimental results of Kupfer at el. [VIII] in terms of stress-strain curves in Fig. 10. Predicted curves compared well with the experimental curves both in terms of peak stress and strains. It can be noted that as σ_1/σ_3 is getting smaller, $\sigma_3/f_c^{'}$ approaches unity or that the T-C model degenerates to the uniaxial compression case.

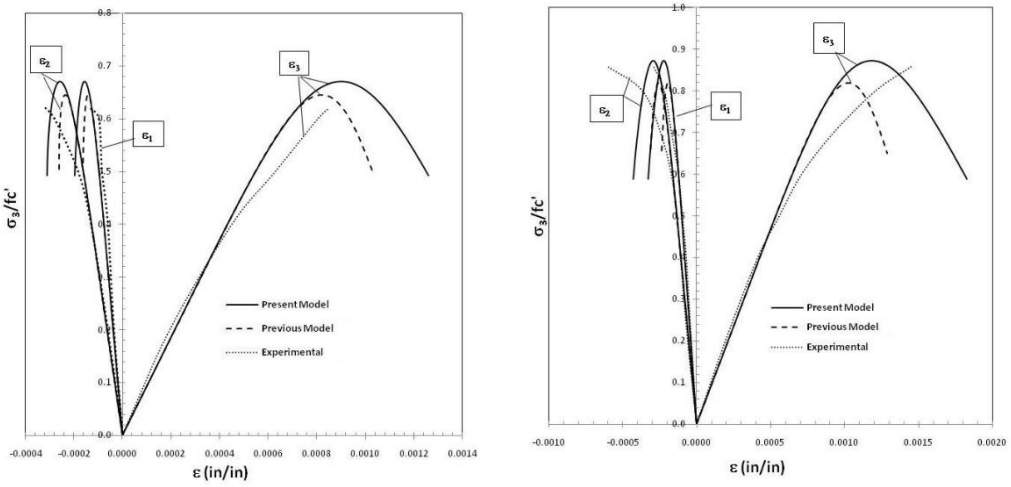

Figure 10. Stress-Strain Curve for Combined Tension-Compression ($\sigma_1/\sigma_3 = -.103$, $\sigma_2/\sigma_3 = 0$ and $\sigma_1/\sigma_3 = -0.052$,$\sigma_2/\sigma_3 = 0$)

Tension Compression Compression (T-C-C): For the case of tension-compression-compression, predictions are compared with the experimental results of Linhua*et al.*[XII] in terms of peak stress (Fig. 11). It can be seen that, in general the predictions in terms of peak stress are compatible with the experimental results of Linhua*et al.*[XII] except in the range of small or zero tensile stresses. For small tensile stresses, the predictions are on the higher side, while for the case of zero tensile stresses i.e., biaxial compression, the predictions are on the lower side. For the case of biaxial compression, it can be attributed to the fact that model is calibrated using the experimental results of Kupfer at el. [VIII] which are on lower side of Linhua*et al.*[XII].

Stress strain curves Figs. 12 and 13, show the same trend as observed for the case of peak stress i.e. they compare well with the experimental curves [XII] in general except for the case of small tensile stresses. Also, it can be observed that predicted compressive strain are more compatible with the experimental compressive strains than tensile strains which are higher as compared to the predicted strains almost in all cases. The difference is due to unavailability of the values of initial young's modulus and Poisson's ratio from the experimental data which play important role in calibration of α and $\beta$and lateral strains.

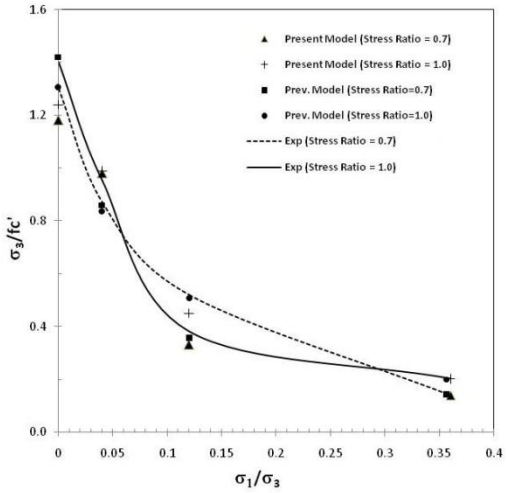

Figure 11. Comparison of T-C-C Results in Terms of Peak Stresses

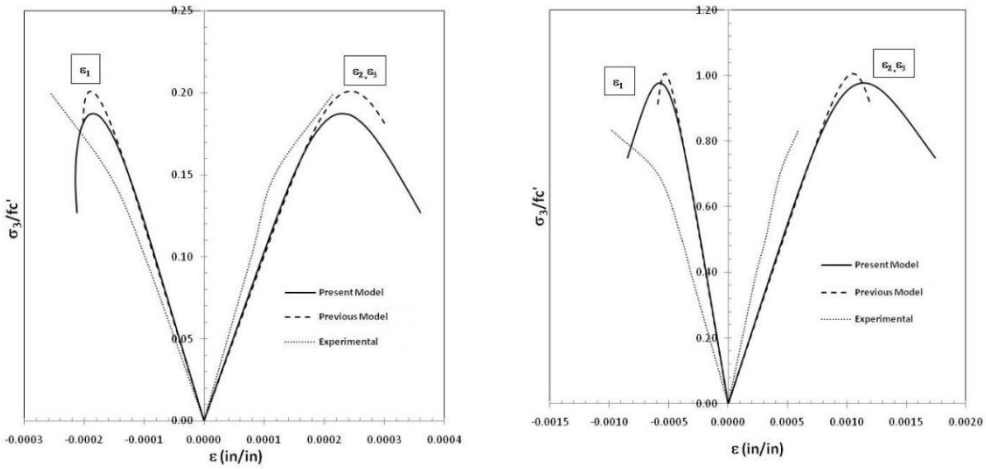

Figure 12**.** Stress-Strain Curve for Concrete under T-C-C ($\sigma_1/\sigma_3 = -0.357, \sigma_2/\sigma_3 = 1$ and $\sigma_1/\sigma_3 = -0.04, \sigma_2/\sigma_3 = 1$)

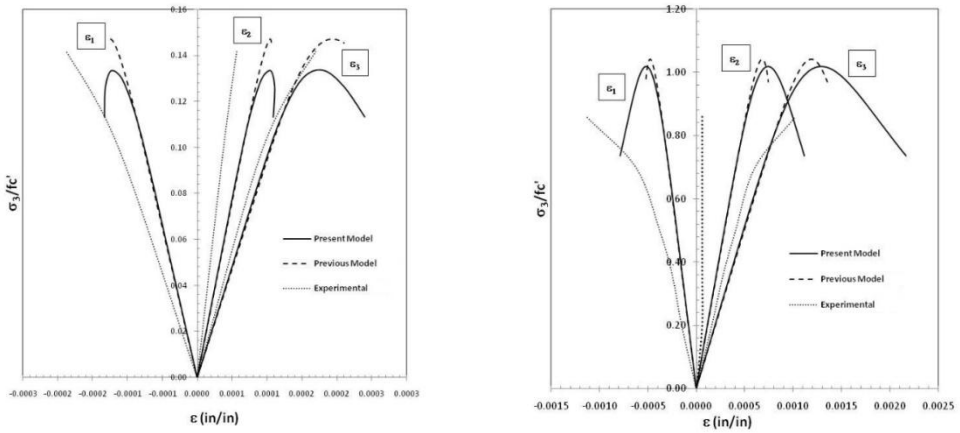

Figure 13**.** Stress-Strain Curve for Concrete under T-C-C ($\sigma_1/\sigma_3 = -0.357, \sigma_2/\sigma_3 = 0.7$ and $\sigma_1/\sigma_3 = -0.04, \sigma_2/\sigma_3 = 0.7$)

Damage Accumulation

Accumulation of damage for concrete under uniaxial compression is presented for Concretes A, B and C in Fig. 14 with respect to movement of loading surface f i.e. the magnitude of strain energy release vector R_i and $\sigma_3/f_c^{'}$. In Fig. 14 damage accumulation curves are compared with those of previous model [I]. It can be noticed from Fig. 14 that predicted curves are not overlapping in contrast to the previous curves where all the curves are overlapping. This is due to the fact that the critical strain energy release rate R_c and damage modulus H and are no more constants and are now functions of compressive strength and elastic modulus of concrete like other parameters α, β and γ. It is obvious from Fig. 14 that the damage modulus H is still infinite at the beginning and becomes zero at failure like previous model. Higher accumulation of damage can also be noticed for present model in Fig. 14 as compared to previous model. This is again due to the dependency of critical strain energy release rate R_c on compressive strength and modulus of elasticity of concrete.

V. Conclusions

An elasto-damage model developed by Khan *et al.* [I] and modified for biaxial states of stress by Khan and Naseem [II] to model monotonic behavior of normal and high strength concretes was further improved. Generalized effective compliance matrix in the principal coordinate system, proposed by Khan *et al.* [I], and critical strain energy release rate, R_c, defined as a function of elastic modulus and uniaxial compressive strength by Khan and Naseem [II], is used. Following are the main conclusions drawn from the study:

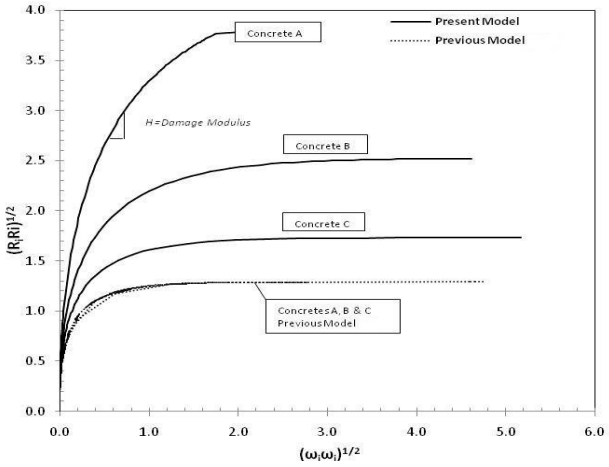

Figure 14. Damage Accumulation Vs. $(R_i R_i)^{1/2}$ for Concretes A, B & C under Uniaxial Compression

1. Proposed form of critical energy release rate R_c by Khan and Naseem [II] was adopted in the present study which resulted in new estimates of the model parameters α, β and γ. Proposed form of R_c and new estimates of parameters are shown to have improved overall performance of the model reflected by the comparisons made with experimental data available in literature and that of previous model by Khan *et al.*[I].
2. Stress-strain curves predicted by the present model have shown better post peak behavior as compared to the previous model and are in good agreement with the experimental curves. This is attributed to the definition of critical energy release rate as a function of elastic modulus and compressive strength of concrete.
3. Proposed model predicts the behavior of concrete under triaxial loadings adequately and captures almost all the essential features of concrete including stiffness degradation, strain softening, volumetric dilatation, different behavior in tension and compression, and gain in strength under increasing confinement.
4. Predicted behavior of concrete subjected to non-proportionate loading is shown to be comparable with the available experimental results. Predicted response, especially when concrete is subjected to non-proportionate triaxial compressive loading, can be improved by calibrating model parameter β against more experimental data at high confining pressures.

Acknowledgement

The work presented in this paper was supported by NED University of Engineering and Technology, Karachi, Pakistan without which it was not viable.

References

I. A.R.Khan, A.H.Gadhib, M.H.Baluch, "Elasto-damage model for high strength concrete subjected to multiaxial loading", International Journal of Damage Mechanics; Vol. 16, pp. 361-398, July 2007.

II. A.R.Khan, N.Naseem, "Damage model for normal and high strength concrete". In Proceedings of Concrete Modelling (CONMOD '08), Delft, The Netherlands, 26-28 May, 2008.

III. C.Z.Wang, Z.H.Guo, X.Q.Zhang, "Experimental investigation of biaxial and triaxial compressive concrete strength", ACI Materials Journal, Vol. 84, pp. 92–100, 1987.

IV. D.C.Candappa, J.G.Sanjayan, S.Setunge, "Complete triaxial stress-strain curves of high-strength concrete", Journal of Materials in Civil Engineering, Vol.: 13, Issue: 3, 209–215, 2001.

V. D.Sfer, I.Carol, R.Gettu, "Study of the behaviour of concrete under triaxial compression", Journal of Engineering Mechanics, ASCE, Vol.: 128, Issue: 2,pp. 156-163, 2002.

VI. G.Wischers, "Applications of effects of compressive loads on concrete". BetonTechnischeBerichte No 2 and 3, Duesseldorf, Germany. 1978.

VII. G.Z.Voyiadjis, J.M.Abu-Lebdeh, "Plasticity model for concrete using the bounding surface concept", International Journal of Plasticity; Vol.: 10, pp. 1-21, 1994.

VIII. H.B.Kupfer, H.K.Hildrof, H.Rusch, "Behavior of concrete under biaxial stresses", Proc ACI, Vol.: 66, Issue: 8, pp.656-666, 1969.

IX. H.C.Wu, C.Komarakulnanakorn, "Endochronic theory of continuum damage mechanics", Journal of Engineering Mechanics, ASCE; Vol.: 124, Issue: 2, 200-208, 1998.

X. I.Imran, J.Pantazopoulou, "Experimental study of plain concrete under triaxial stress", ACI Materials Journal, Vol.: 93, Issue: 6, pp. 589–601, 1996.

XI. J.Lee, G.L.Fenves, "Plastic-Damage model for cyclic loading of concrete structures", Journal of Engineering Mechanics, ASCE, Vol. 124, Issue: 8, pp. 892-900, 1998.

XII. J.Linhua, H.Dahai, X.Nian Xing, "Behavior of concrete under traixial compressive-compressive -tensile stresses", ACI Materials Journal, Vol.; 88, Issue: 2, pp. 181-185, 1991.

XIII. M.Attard, S.Setunge, "Stress-strain relationship of confined and unconfined concrete", ACI Materials Journal, Vol.: 93, Issue: 5, pp. 433–442, 1996.

XIV. R.R.Babu, G.S.Benipal, A.K.Singh, "Constitutive modeling of concrete: An overview", Asian Journal of Civil Engineering (Building and Housing), Vol.:6, Issue: 4, pp. 211-246, 2005.

XV. S.H.Ahmad, S.P.Shah, "Complete triaxial stress-strain curves for concrete", Proc. ASCE, Vol.: 108, Issue: 4, pp. 728–742, 1982.

XVI. T.Gabet, X. H.Vu, Y.Malecot, L.Daudeville, "A new experimental technique for the analysis of concrete under high triaxial loading", Journal de Physique IV, Vol.: 134, pp. 635-640, 2006.

XVII. T.Hampel, K.Speck, S.Scheerer, R.Ritter, M.Curbach, "High-performance concrete under biaxial and triaxial loads", Journal of Engineering Mechanics, ASCE, Vol.: 135, Issue: 11, pp. 1274-1280, 2009.

XVIII. T.H.Wee, M.S.Chin, M.A.Mansur, "Stress-strain relationship of high-strength concrete in compression", Journal of Materials in Civil Engineering, ASCE, Vol.: 8, Issue: 2, pp. 70-76, 1996.

XIX. V.S.Gopalratnam, S.P.Shah, "Softening response of plain concrete in direct tension", Proc. ACI,Vol.: 82, Issue: 3, pp. 310-323, 1985.

XX. W.F.Chen, Constitutive Equations for Engineering Materials, Vol. 1: Elasticity and Modelling, Elsevier Publications, 1994.

XXI. W.P.Lokuge, J.G.Sanjayan, S.Setunge, "Stress strain model for laterally confined concrete", Journal of Materials in Civil Engineering, ASCE; Vol.: 17, Issue: 6, pp. 607–616, 2005.

XXII. W.Suaris, C.Ouyang, V.M.Fernando, "Damage model for cyclic loading of concrete", Journal of Engineering Mechanics, ASCE, Vol. 116, Issue: 5, pp. 1020-1035, 1990.